A&A manuscript no.
(will be inserted by hand later)

Your thesaurus codes are:
08 (08.09.2 β Pic; 08.03.4; 08.16.2; 03.13.4)

ASTRONOMY
AND
ASTROPHYSICS
1.2.2008

Dust distribution in disks supplied by small bodies: Is the β Pictoris disk a gigantic multi-cometary tail?

A. Lecavelier des Etangs[1], **A. Vidal-Madjar**[1], **and R. Ferlet**[1]

Institut d'Astrophysique de Paris, 98 Boulevard Arago, F-75014 Paris, France

Received; accepted

Abstract. We have evaluated the spatial distribution of dust in disks supplied by colliding or evaporating bodies spread in a small belt. The gradient of the distribution of dust expelled by radiation pressure is generally steeper than the one observed around βPictoris. It follows that, to generate the βPictoris disk distribution in such a way, one should extract relatively more small particles in the production process: thanks to radiation forces, these smaller particles have large eccentricities and thus could be seen at very large distances from their injection place. The evaporation process of comet-like bodies moving slowly inwards may yield the necessary particle size distribution.

It is interesting to note that this dynamical description is able to account for the main observational properties of the β Pictoris disk, such as the power law distribution with possibly a change in slope, the asymmetry at large distances, and the total mass, all of which have remained unexplained up to now. If confirmed, this scenario may indicate that the β Pictoris disk could be looked on as a gigantic multi-cometary tail with its natural constituents: gas and dust.

Key words: stars: β Pic – circumstellar matter – planetary systems

1. Introduction

Since the discovery of the dusty disk around β Pictoris (Aumann 1984, Smith & Terrile 1984), it has been the subject of extensive investigations with all possible observational techniques: visible and IR imagery (Smith & Terrile 1987, Paresce & Burrows 1987, Lecavelier des Etangs et al. 1993, Golimowski et al. 1993, Lagage & Pantin 1994), spectroscopy (Vidal-Madjar et al. 1994, Vidal-Madjar & Ferlet 1995 and references therein) and recently photometric variations (Lecavelier des Etangs et al. 1995). In particular, the stellar light scattered by dust particles has been well observed by several authors for many years to follow a power law distribution with a slope in the range -3.6 (Artymowicz et al. 1989, Lecavelier des Etangs et al. 1993) -4.3 (Smith & Terrile 1984). However, a convincing explanation for this scattered light distribution is still needed.

The dust distribution in the β Pictoris disk may be a crucial issue for understanding its origin. We present here a precise dynamical model which will be compared with the observations for the first time in a quantitative manner.

Another key point revealed by the spectroscopic studies of the gaseous counterpart of the β Pictoris disk is the existence of orbiting kilometer size bodies which sometimes fall onto the star, giving rise to the observed spectroscopic redshifted signatures due to ejected gas, and undoubtedly to dust particles. Already in 1984, Weissman (1984) questioned whether the material around Vega-like stars is of cometary or asteroidal origin and suggested that particles could be continually supplied by sublimation or from collisions between larger bodies.

The time scale evaluation over which dust particles are eliminated by the Poynting-Robertson effect or collisions (Backman & Paresce 1993) leads to durations much shorter than the estimated age of βPictoris ($\sim 2{\cdot}10^8$ years according to Paresce, 1991). This simple comparison suggests convincingly that the βPictoris disk is not a remnant of planetary formation but on the contrary must be continually replenished by secondary sources like evaporation or collision of small bodies. This seems in fact a very natural hypothesis (see for example Zuckerman & Becklin 1993): the presence of small bodies is a consequence of planetary systems formation (Lissauer 1993).

Furthermore, CO absorptions have been recently observed towards β Pictoris (Vidal-Madjar et al. 1994) with the Hubble Space Telescope. The very presence of CO may also require a permanent source provided by evaporation of comet-like bodies.

Send offprint requests to: A. Lecavelier des Etangs

Here we present a new argument: This replenishment is able to reproduce the main characteristics of the βPictoris dust disk, and in particular the spatial distribution of dust at large distances. In detail, it gives possible explanations for the following unexplained issues:

1. The gradient of the scattered light follows a relatively well-known but unexplained power law (e.g. Golimowski et al. 1993).
2. The distribution at large distances is obviously not axisymmetric (Smith & Terrile 1987, Kallas & Jewitt 1995).
3. The central part of the disk is relatively clear of dust (Backman et al. 1992, Lagage & Pantin 1994).
4. The disk seems to be a "wedge" disk: the thickness increases with radius (Backman & Paresce 1993, Lecavelier des Etangs et al. 1993).
5. The slope of the scattered light distribution changes abruptly at about 100 AU from the star. If confirmed, this fact remains unexplained (Artymowicz et al. 1990, Golimowski et al. 1993).

Furthermore, the possible explanation of these observational facts could give new understanding to the following questions:

– a) What is the mass of the dust disk, since when extrapolated towards infinite distances the disk mass diverges (Artymowicz et al. 1989)?
– b) Are there connections between the dust and the gas disks ?
– c) Can the asymmetry in the observed dust disk be connected with the asymmetry in the longitude of periastron of the comets in the Falling-Evaporating-Bodies (FEB) model proposed to explain the redshifted spectroscopic events (e.g. Beust et al. 1991)?

Therefore, we will consider here a model in which the disk is replenished by a group of kilometer-size bodies (Section 2). Numerical calculations of the spatial distribution of dust are given in Section 3. We shall discuss in Section 4 the β Pictoris disk in such a scenario and summarize the results in Section 5.

2. The model

2.1. Basic concept

We assume that the dust is produced by cometary or asteroid-like bodies which create particles through mutual collisions or evaporation processes. The main assumption is thus that these particles have small initial velocities relative to the parent bodies: less than 1 km/s like in cometary production (Gombosi et al. 1985, Sekanina 1987) or in "Chiron burst" (Luu & Jewitt 1990). Thus, these velocities can be considered as negligible in comparison to the orbital velocities. In our model, this relative velocity is fixed at zero. However, as soon as a dust particle is ejected, it is perturbed by the radiation pressure; its orbit is different from the parent body one and tangent at the point where it was injected (Burns et al. 1979). For example, if a parent body in a circular orbit with a semi-major axis a_0 produces a particle with a ratio β of the radiation force to the gravitational force, the particle orbit has a semi-major axis $a_\beta = a_0(1-\beta)/(1-2\beta)$ and an eccentricity $e_\beta = \beta/(1-\beta)$. The periastron is $a_\beta(1-e_\beta) = a_0$ and the apoastron $a_\beta(1+e_\beta) = a_0/(1-2\beta)$.

Therefore, particles can be observed at distances from the central star much larger than the apoastron of the parent body. Thus, local perturbations on the distribution of the parent bodies like asymmetries, could produce observable signatures on the dust distribution at very large distances.

2.2. Particle size distribution

Furthermore, because the parent bodies should not produce single sized particles, we introduce in the calculation a size distribution. For particles with radius $s \geq 1\mu$, β is correlated with the size of the particle by $\beta \sim s^{-1}$ (Artymowicz 1988). We can assume a power law size distribution as in Solar System cometary dust (Lien 1990 and references therein), in collisionally replenished dust (Greenberg & Nolan 1989), or in interplanetary medium dust (Le Sergeant & Lamy 1980). Thus, if we have a size distribution $dn \propto s^q ds$, then we have $dn \propto \beta^K d\beta$ with $K = -q-2$.

2.3. Analytical consideration

2.3.1. One point production

First, let us consider a parent body in a circular orbit which generates a set of particles at a given point. Then the particles with $\beta > 0.5$ have hyperbolic orbits and are ejected from the system towards the interstellar medium. The other particles with $\beta < 0.5$ follow orbits within a parabola which is the orbit of the particles with $\beta = 0.5$.

One can evaluate the surface density of particles in the asymptotic direction of the parabola: for a given particle the true anomaly θ follows the distribution law

$$P_\theta(\theta)d\theta = \frac{(1-e)^{3/2}}{2\pi(1+e\cos\theta)^2}d\theta \qquad (1)$$

In the asymptotic direction $\theta = \pi$, $P_\theta(\pi) \propto (1-e)^{-1/2} \propto r^{1/2}(1+a_0/r)^{1/2}$. The probability that the particle apoastron is between r and $r+dr$ in the same direction is $P_r(r) = \beta^K(d\beta/dr)dr$. Since $\beta = (1-a_0/r)/2$, $P_r(r) \propto (1-a_0/r)^K r^{-2}dr$. Thus, taking into account the scattering cross section $\sigma \propto \beta^{-2}$ we obtain the surface density normal to the plane of the disk $\sigma \cdot n_s$:

$$\sigma \cdot 2\pi r \cdot n_s(r) \propto r^{-3/2}(1-a_0/r)^K(1+a_0/r)^{1/2} \qquad (2)$$

Thus $\sigma \cdot n_s(r)_{r\to\infty} \propto r^{-2.5}$.

2.3.2. Parent bodies in circular orbits.

However, dust production can take place at every point in the orbit of the parent body. Here, we restrict ourselves to a parent body in circular orbit, thus, producing an axisymmetrical disk. Each particle has a probability $f_\beta(r)$ to be at a distance r: $f_\beta(r) \propto ((1-a_0/r)(2\beta-1+a_0/r))^{-1/2}$. The surface density normal to the plane of the disk is then:

$$\sigma \cdot n_s(r) \propto \int_{(r-a_0)/2r}^{1/2} \frac{\beta^{K-2} f_\beta(r) d\beta}{2\pi r \int_{a_0}^{a_0/(1-2\beta)} f_\beta(r_1) dr_1} \qquad (3)$$

This surface density follows an r^{-3} law and is plotted in Fig. 1.

Moreover, the inclination of the particles is the same as the inclination of the parent bodies. Therefore, the vertical distribution of the particles depends on the distribution of the inclination of the parent bodies. In the present model the thickness of the disk is increasing with radius and the volume density (n_v) is proportional to the surface density (n_s) divided by the distance, i.e. $n_v(r) \propto r^{-4}$.

It has to be noted that this conclusion is valid at distances larger than the distance of the farthest parent bodies. Within this zone the opening angle must look smaller.

From the $n_v(r) \propto r^{-4}$ law and Nakano's (1990) conclusion concerning the connection between the volume density and the scattering light distribution ($F(r) \propto n_v(r)/r$), one can conclude that a belt of parent bodies in circular orbits should produce a "wedge" disk with a scattered light distribution $F(r) \propto r^{-5}$.

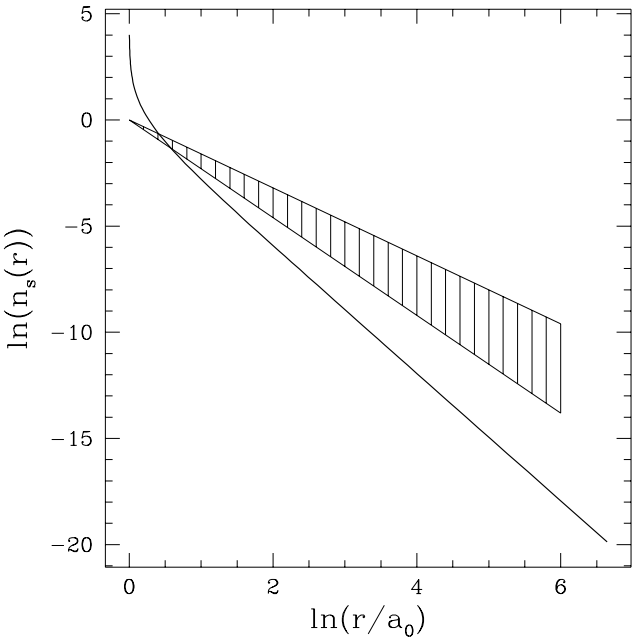

Fig. 1. Plot of the surface density distribution calculated from Eq. 3. The abrupt density decrease at $r \sim a_0$ is simply due to the assumed single distance between the central star and all the parent bodies. It is thus an artificial consequence of an oversimplified hypothesis.
For comparison, the hatched zone represents the distribution range of slopes deduced by different observers around β Pictoris.

3. Numerical results

3.1. The Monte-Carlo simulation

The analytical model of the previous section can only be solved for a limited number of parameters and parent body distributions. We have chosen to evaluate the dust distribution by a Monte-Carlo method. We shall consider a given family of parent bodies, a dust production law and a particle size distribution, and we shall integrate the distribution in the following way:

For each of the N random particles, we first randomly select a parent body in the family and its position in its orbit; then we randomly apply the particle size distribution and we calculate the position r_i of the particle i after a time t where t is randomly chosen between 0 and t_{max}. Finally, we evaluate $F(r)$ the surface brightness along the midplane of the edge-on disk projected on the sky at the projected distance r. If $F_i(r)$ is the contribution of the particle i, from Eq. 2 of Nakano (1990), we have

$$F_i(r) \propto r^{-1} \int_0^\pi n_i(\Lambda) \sigma_i(\theta) d\theta \qquad (4)$$

where Λ is the distance to the central star and $\sigma_i(\theta)$ is the scattering phase function. Nakano (1990) has already shown that, except if the dust is much more steeply forward-scattering than in the Solar System, the isotropic scattering assumption does not change the observed slope of the scattered light distribution, thus $\sigma_i(\theta) = \beta_i^{-2}$ with $\sin\theta = r/\Lambda$. The volume density is given by $n_i(\Lambda) = \delta(\Lambda - r_i) \cdot p_i/r_i$ where p_i is the production rate of dust on the parent bodies, then $F_i(r) \propto r^{-1} \int \delta(\Lambda - r_i) p_i \mathrm{H}(\Lambda - r) r d\Lambda / (r_i \beta_i^2 \Lambda \sqrt{\Lambda^2 - r^2})$ where H is the Heavyside function.

Finally, the surface brightness at a given projected distance r from the star is estimated by

$$F(r) = \sum_{i=1}^{N} F_i(r) \propto \sum_{i=1}^{N} \frac{\mathrm{H}(r_i - r) \cdot p_i}{r_i^2 \sqrt{r_i^2 - r^2} \cdot \beta_i^2} \qquad (5)$$

3.2. Results

Results of runs with different initial conditions on the family of parent bodies are summarized in Tables 1 and 2. The production rates per annulus of fixed width are given for each run. Several configurations have been tried. The first one corresponds to the analytical model of Sect. 2.3.2, we find again $\alpha = 5.0$, which validates the Monte-Carlo model. In runs #2 and #3, we have tried different distances and evolutionary times which show that the Poynting-Robertson effect does not change the results:

the accuracy for α is about 0.1. From #4 to #11, the parent bodies are in eccentric orbits with eccentricities uniformly distributed between 0 and 0.5 or between 0 and 1; it seems that bodies with eccentricities larger than 0.5 do not contribute much to the distribution since a large fraction of ejected material is then on hyperbolic orbits. In runs #4 to #7, we have taken parent bodies with a peculiar longitude of periastron (ω), namely 155^o. This value has been selected according to the Beust et al. (1991) modelisation of the Falling-Evaporating-Bodies, the so-called FEB scenario needed to reproduce the spectroscopic redshifted signatures. In the four last runs of Table 1, ω was uniformly distributed between 0^o and 360^o.

From all the results in Table 1, it can be seen that the slope α is always greater than or equal to 5.0. In Table 2, we test other parent body distributions in which the dust observed at large distances still is produced close to the star. Incidentally, another solution would be to assume that the disk is produced by a distribution of asteroids up to 1000 AU from the star. However this solution does not allow us to explain the observed asymmetries.

Runs # 12 to # 15 take into account the Epstein gas drag with a gas density $\rho_{gas} = \rho_0(100 \text{ AU}/r)$ and temperature $T_{gas} = 20$ K. Runs # 16 and # 17 are with dust size distribution characterized by $K = 5 - 10$.

4. The β Pictoris disk

4.1. Orbiting-Evaporating-Bodies (OEB). Towards a solution?

The observed distribution in the external part of the β Pictoris disk ($\alpha \leq 4.3$) is less steep than all calculated slopes in Tables 1. It has to be noted that a solution compatible with the observed slope could be obtained with a gas density $\rho_0 \sim 10^5$ cm^{-3} at 100 AU. However, this is excluded by the upper limit deduced from spectroscopic or HI observations (Vidal-Madjar et al. 1986, Freudling et al. 1995).

Runs #16 and #17 are also compatible with the dust distribution in β Pictoris (Fig. 2). But they require dust size distributions ($K = 5 - 10$) very different from the expected ones if they are produced through collisions between parent bodies (Fujiwara 1979 and references therein). However they show us that we need a relatively larger amount of smaller particles which have larger apoastrons.

In the evaporation process of large bodies (like Chiron), there is an upper limit s_{max} to the size of the ejected particles extracted by gas (Luu & Jewitt 1990). Following Cowan & A'Hearn (1982) we have calculated this upper limit and the evaporation rate Z in molecules per second per unit area for CO and CO_2 as a function of the distance to β Pictoris, assuming $L_{\beta Pic} = 6L_\odot$ and a typical parent body radius $R_{body} = 100$ km (Figs. 3 and 4). This upper limit is inversely proportional to the parent body size R_{body}.

We have introduced this effect in our model. The results are summarized in Table 3 for CO_2; they would be similar for CO if the parent bodies were at larger distances. Here, we have taken the production rate $p \propto Z \cdot R_{body}^2$ and a parent bodies size distribution $dn = R_{body}^{-\gamma} dR_{body}$ where $\gamma = 3.5$ (uncertainties deduced from observations in the Solar System with γ between 3.2 (Whipple 1975, Hughes & Daniels 1982) and 3.8 (Fernández 1982) do not change the present results).

In runs # 101 to # 103, we take a wide belt of parent bodies from 15 to 30 AU, without correlation between their radius R_{body} and their distance from the central star. We obtain $\alpha \sim 4.8 - 4.9$; the effect of cutoff in particle size is not efficient enough to explain the observed slope $\alpha \sim 3.6 - 4.3$.

However, if the evaporating bodies are coming from larger distances and their orbital parameters diffuse from a Kuiper belt-like zone towards a planetary-like zone, the smaller parent bodies lost their volatile material very early at larger distances whereas the larger bodies can evaporate downward at smaller distances.

This scenario can be modelized in the following way: a parent body with a characteristic distance (which can be the periastron or the semi-major axis) $r(t) = r_0 - \dot{r}t$ is considered as evaporating at $r = r(T)$ only if the total mass of the previously evaporated gas is smaller than the available mass of volatile material.

$$\int_0^T \mu Z(r(t)) 4\pi R_{body}^2 \lambda dt < \frac{4\pi}{3} \rho \xi R_{body}^3 \quad (6)$$

where λ is the percentage of active surface of the body, ξ the relative mass of CO_2 in the parent body, ρ its density and μ the CO_2 molecular weight. Eq. 6 can be reduced to $R_{body} \geq R_{ref} \int_r^\infty Z(l)dl / \int_{r_{ref}}^\infty Z(l)dl$ where R_{ref} is the reference size of the smallest body which can evaporate at $r = r_{ref}$. For CO_2 evaporation and $r_{ref} = 20$ AU, one obtain

$$\dot{r} = 6 \cdot 10^{-7} \frac{\lambda}{\xi\rho} \left(\frac{10\text{km}}{R_{ref}} \right) \text{AU year}^{-1} \quad (7)$$

In runs # 104 to # 115, only those with $R_{ref} \sim 30 - 40$ km give the observed slope range. Moreover, due to the particle size cutoff, $\beta \geq 0.4$ there is an abrupt break in the slope at $r_{break} \approx a_0/(1 - 2\beta_{min}) \approx 100$ AU (see Fig. 5 for run #106). For CO, one can obtain $\dot{r} = 6 \cdot 10^{-6} \lambda/(\xi\rho)$AU year^{-1}, and there would be also an abrupt break in the slope since CO begins to evaporate from about 100-150 AU.

4.2. Discussion

We saw in the previous section that the observed gradient in the β Pictoris disk can be explained by the present

Table 1. Slope α of the gradient of brightness in disks with different conditions for the parents bodies. In all these runs we assumed N=10000 and K=1.5. Poynting-Robertson drag is taken into account but there is no gas drag. For runs # 4 to # 7, the two slopes are for the both sides of the asymmetrical disk seen from the Earth.

Run	Parent Bodies Parameters				t_{max}	Result: α
#	semi-major axis (AU)	Eccentricity	ω	Production rate	(years)	$F(r) \propto r^{-\alpha}$
1	20	0.	-	$p = const$	10000	5.0
2	2	0.	-	$p = const$	10000	4.9
3	20	0.	-	$p = const$	100000	5.0
4	20-30	0.-0.5	155^o	$p = const$	10000	5.2-5.6
5	20-30	0.-1.	155^o	$p = const$	10000	5.2-5.7
6	20-30	0.-0.5	155^o	$p \propto r^{-3}$	10000	5.3-5.5
7	20-30	0.-1.	155^o	$p \propto r^{-3}$	10000	5.3-5.6
8	20-30	0.-0.5	0-360^o	$p = const$	10000	5.2
9	20-30	0.-1.	0-360^o	$p = const$	10000	5.3
10	20-30	0.-0.5	0-360^o	$p \propto r^{-3}$	10000	5.2
11	20-30	0.-1.	0-360^o	$p \propto r^{-3}$	10000	5.4

Table 2. Same as the previous table, with different K; gas drag is taken into account. The parent bodies have semi-major axis a =20 AU and eccentricity $e = 0$. t_{max}=10000. For the runs # 16 the slope gradually changes from $\alpha = 3.7$ at 20 AU to $\alpha = 4.7$ at 800 AU; and for run # 17 from 2.9 to 4.4 respectively.

Run	β distribution:K	gas density at 100 AU	Result: α
#	$dn = \beta^K d\beta$	(cm^{-3})	$F(r) \propto r^{-\alpha}$
12	1.5	100.	5.0
13	1.5	1000.	5.1
14	1.5	10000.	4.6
15	1.5	100000.	3.8
16	5.	0.	3.7-4.7
17	10.	0.	2.9-4.4

model only if there is a larger amount of small particles. Now, there is an upper limit in the size of particles ejected by slowly evaporating bodies due to a balance between gas drag and gravitation. In fact, we obtain dust disks very similar to the β Pictoris one by assuming evaporation of kilometer size bodies which are diffusing from a Kuiper belt-like zone inward an evaporation zone.

The time scale $\dot{r} \sim 10^{-7}$ AU year^{-1} in the diffusion of comet orbital elements, which is necessarily to explain β Pictoris's characteristics, is consistent with the few AU in 10 Myr deduced by Torbett & Smoluchowski (1990) and Levison's (1991) results on the Kuiper belt dynamical behavior between 30 and 40 AU around the Sun. The analysis of the evolution of the orbital elements of the parent bodies is outside the scope of this paper; moreover, the motion of such Kuiper belt-like bodies under the influence of a planetary system is probably chaotic (Scholl 1979, Torbett & Smoluchowski 1990) and very dependent on this planetary system. The present model merely shows us that the dust distribution may be an important clue and may be explained by the present model if there is a long time scale perturbation of parent bodies by a planetary system which is compatible with the one predicted for the Solar System.

Another evolution process for heating the bodies consists in the increase of the star luminosity (L) during its evolution along the main sequence. For a star of 1.6 $\mathrm{M}_\odot$, we have $dL/Ldt = 2 \cdot 10^{-10}$ year^{-1}, if $\tilde{r}$ is the distance of equal luminosity, this corresponds to $\dot{\tilde{r}} = \tilde{r}/2L \cdot dL/dt$. This solution would have the advantage of being "planetary system" independent. However, if the primary volatile is CO, $\dot{\tilde{r}} = 10^{-8}$ AU year^{-1}; even if the volatile is CO_2, $\dot{\tilde{r}} = 2.5 \cdot 10^{-9}$ AU year^{-1}. The time scales do not seem to be adequate. This mechanism would be efficient only if we could have bodies with very large quantities of volatiles and very small fractions of active surface.

The assumption that CO or CO_2 can be primary volatiles is not a problem since around an AV star they can evaporate at very large distances where the presence of young objects without a lag deposit of nonvolatile forming a crust is likely. On the contrary in the Solar System, we observe bright comets only when H_2O can evaporate, simply because CO or CO_2 evaporate only inside planetary regions where, for dynamical reasons, the presence of young objects is unlikely: Chiron seems to be an exception but provides a useful analogy with what may happen around β Pictoris.

Table 3. Same as the previous tables, for particles ejected by evaporating gas. Here we assume that the gas is CO_2 and $p \propto Z \cdot R_{body}^2$. R_{ref} is the radius of the largest dead comets at r_{ref}=20 AU. For runs # 105 to # 115 there is a slope break at $r = r_{break}$, and both inward and outward slopes α_{in} and α_{out} are given. For runs # 113 to # 115 the two given slopes α_{in} are for each side of the disk. We always took t_{max}=10000 years.

Run	Parent Bodies Parameters			R_{ref}	Result:		$F(r) \propto r^{-\alpha}$	Brightness
					r_{break}	α_{in}	α_{out}	ratio
#	Periastron (AU)	Eccentricity	ω	(km)	(AU)			
101	20-30	0.	-	-	-	-	4.8	-
102	20-30	0.-0.5	0-360^o	-	-	-	4.9	-
103	20-30	0.-0.5	155^o	-	-	-	4.9	-
104	15-30	0.	-	10.	-	-	4.6	-
105	15-30	0.	-	20.	50	2.9	4.5	-
106	15-30	0.	-	30.	100	2.7	4.3	-
107	15-30	0.	-	40.	180	2.5	3.9	-
108	15-30	0.-0.5	0-360^o	10.	-	-	4.6	-
109	15-30	0.-0.5	0-360^o	20.	50	2.8	4.5	-
110	15-30	0.-0.5	0-360^o	30.	130	2.8	4.3	-
111	15-30	0.-0.5	0-360^o	40.	180	2.6	3.7	-
112	15-30	0.-0.5	155^o	10.	-	-	4.6	2.9
113	15-30	0.-0.5	155^o	20.	50	2.2-4.0	4.5	2.8
114	15-30	0.-0.5	155^o	30.	110	2.7-3.7	4.3	3.5
115	15-30	0.-0.5	155^o	40.	180	2.7-3.4	3.7	4.0

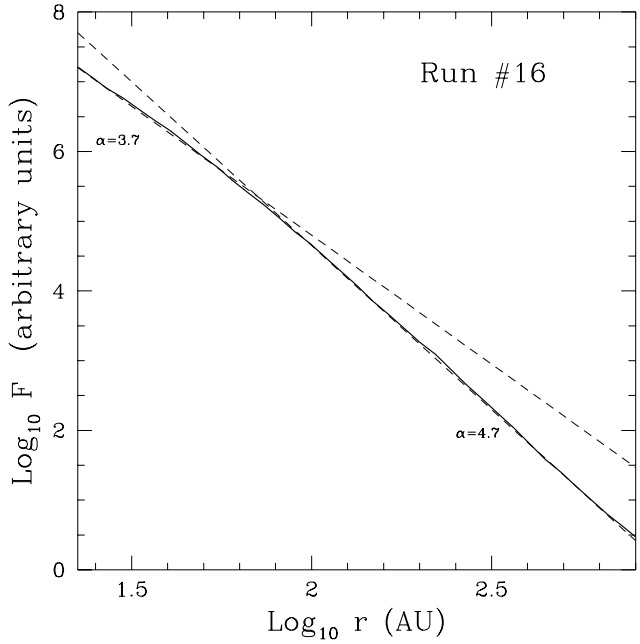

Fig. 2. Plot of the surface brightness (arbitrary unit) of the equatorial plane of an edge-on disk seen from the Earth calculated in run # 16. The slope varies from -3.7 to -4.7. For comparison, the dashed lines represent the power laws $r^{-3.7}$ and $r^{-4.7}$.

As we shall see below, this model is also able to give answers to other important issues defined in Section 1.

4.3. Asymmetry

The distribution observed at large distances in β Pictoris disk is obviously not axisymmetric (Smith & Terrile 1987, Kallas & Jewitt 1995). However, relative keplerian motions should remove such asymmetries: for two particles on circular orbits with semi-major axis a_1 and a_2, the time needed to put them in opposite side is $t \sim 0.4(a_1^{-3/2} - a_2^{-3/2})^{-1}$ years if a_1 and a_2 are in AU. With $a_1 = 100$ AU and $a_2 \geq 400$ AU we have $t \leq 450$ years, an extremely short time compared to the age of the system. Thus, any asymmetry should quickly disappear.

As noted above, it is however possible to find the asymmetry observed between the two extensions of the β Pictoris disk by assuming a peculiar parent body distribution (see Fig. 6). Runs # 112 to # 115 have been obtained with a peculiar longitude of periastron of the parent bodies ($\omega = 155^o$). We found a brightness ratio between the two extensions of the disk ranging from 2.8 to 4.0. This result shows that the observed ratio of SW to NE extension brightness from 1.1 (Lecavelier des Etangs et al. 1993) to 1.5 (Kallas & Jewitt 1995) can be reproduced if there is a small additional proportion of bodies with peculiar longitudes of periastron like in the FEB scenario.

However, there is another way to obtain the observed asymmetry, namely to assume that bodies with different longitudes of periastron move inwards with different velocities. For example, if bodies with a given longitude of periastron move more slowly inward, it produces a fainter disk extension with a steeper brightness gradient in one particular direction (Fig. 7).

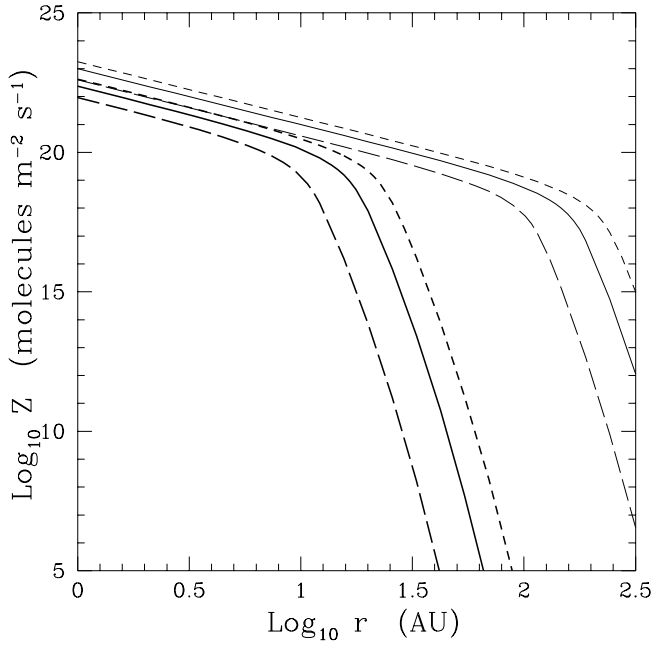

Fig. 3. Plot of the evaporation rate Z as a function of the distance from βPictoris. The thick lines are for CO_2 and the thin ones for CO. The evaporation is calculated for a steady-state energy balance and depends on the albedo A_v of the parent body. The short-dashed lines are for A_v=0.1, the long-dashed are for A_v=0.8 and the solid line are for A_v=0.5. In all the simulations we take A_v=0.5.

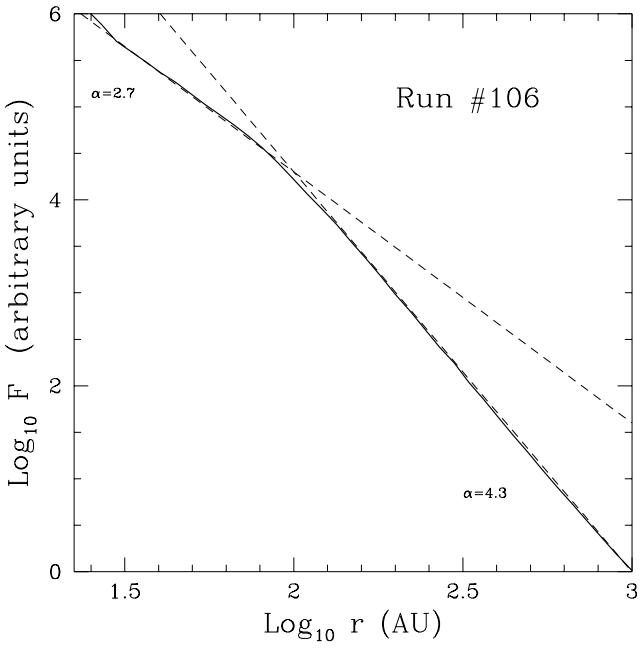

Fig. 5. Plot of the surface brightness $F(r)$ calculated from run # 106. There is an abrupt change in the slope at $r = 100$ AU. The slope is $\alpha = -2.7$ inside and $\alpha = -4.3$ outside this limit. For comparison, the dashed lines represent the power laws $r^{-2.7}$ and $r^{-4.3}$.

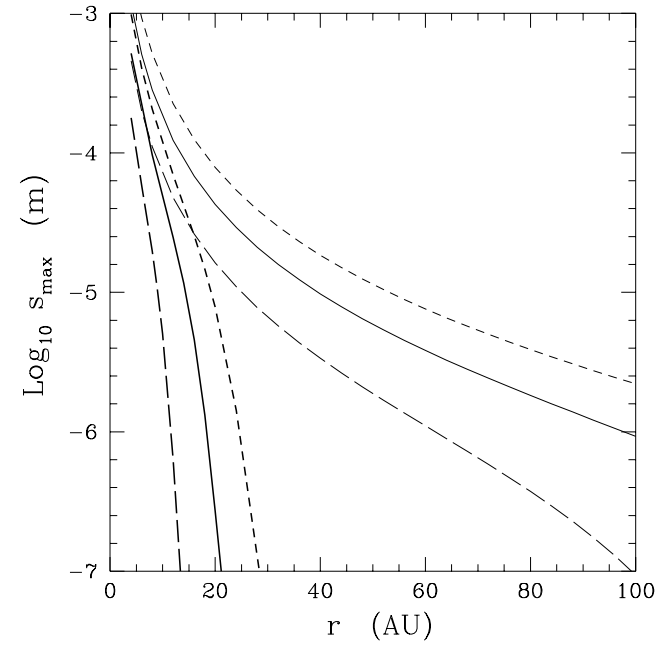

Fig. 4. Plot of the radius of the largest particle which can be ejected from the surface of a parent body with radius R_{body}=100 km and density $\rho_{body} = 1$ as a function of βPictoris distance. The thick lines are for CO_2 and the thin ones for CO. The different albedos A_v are the same as in Fig. 3.

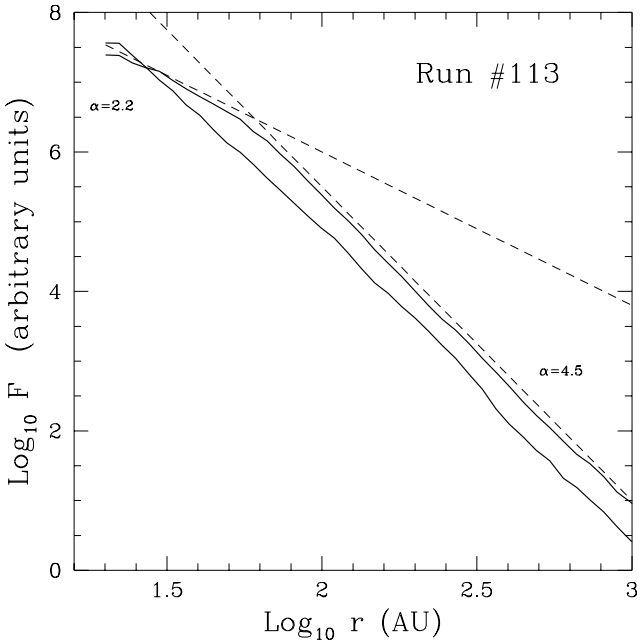

Fig. 6. Plot of the surface brightness of the two extension calculated from run # 113. In this run all the parent bodies have a longitude of periastron of 155^o relative to the line of sight. The brightness ratio between the two extensions is equal to 2.8. For comparison, the dashed lines represent the power laws $r^{-2.2}$ and $r^{-4.5}$.

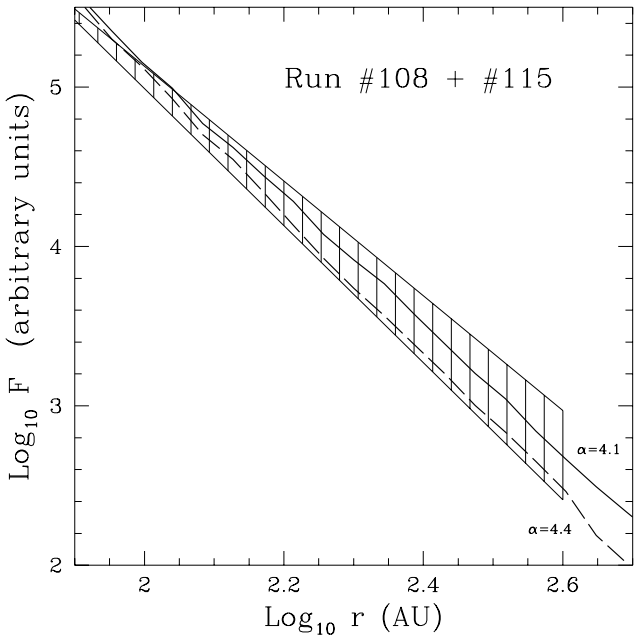

Fig. 7. Plot of the surface brightness calculated from the addition of runs # 108 and #115. In this combined run the parent bodies with a longitude of periastron of 155^o go more slowly inwards. The brightness ratio between the two extensions is equal to 1.3. The fainter extension has a steeper slope and is represented by a long-dashed line.
As in Fig. 1., the hatched zone represents the distribution range of slopes deduced by different observers around β Pictoris.

4.4. Mass of the disk

The total mass of the β Pictoris disk calculated from optical observations is

$$M = \int\int n_s(r,s)\frac{4\pi}{3}\rho s^3 2\pi r dr dn_s \tag{8}$$

where s is the particle size and dn_s the size distribution. As discussed above we can take $dn_s = s^{-3.5}ds$. Previously, authors assumed that s is independent of r the distance from the star. This assumption is the simpler one and others must be justified.

This means however that:

$$M \propto \frac{8\pi^2\rho}{3}\int_{r_{in}}^{r_{out}} n_s(r) r dr \int s^{-0.5} ds \tag{9}$$

The second integral diverges towards the largest bodies; the first one also diverges for $r_{out} \to \infty$ if the slope of the scattering light is ≥ -4 (that is the case according to Artymowicz et al. (1989), Lecavelier des Etangs et al. (1993) and for Golimowski et al.'s (1993) NE extension). Thus to evaluate the mass, an arbitrary limit for the disk extension and particle size must be fixed.

In the framework of our model both problems are directly solved. At a given distance r, we have $2\epsilon \leq s \leq \frac{2\epsilon r}{r-a_0}$ where a_0 is the distance of the parent body to the star and ϵ is defined by $\epsilon = s\beta$. We saw in Section 2.2 that ϵ can be assumed to be constant. We obtain

$$M \propto \frac{4\pi\rho}{3}\int \left(n_s(r) 2\pi r dr \int_{2\epsilon}^{(2\epsilon r)/(r-a_0)} s^{-0.5} ds \right) \tag{10}$$

$$M \propto \frac{16\pi^2}{3}\rho\sqrt{2\epsilon}\int_{r_{in}}^{\infty} n_s(r)\frac{a_0}{2} dr \tag{11}$$

This integral now converges and the computed mass is of the order of few lunar masses, i.e. of the same order as the lower limit evaluated by Artymowicz et al. (1989) who assumed an arbitrary outer limit of 500 AU and single-size particles of 1μ. This mass is consistent with the total mass deduced from submillimeter observations (Zuckerman & Becklin 1993).

4.5. Gas-dust ratio and CO detection.

One can investigate the connection between the dust observed around β Pictoris since 1984 and the gas disk with its stable component thanks to the recent detection of CO in UV lines with the HST ($N_{co} \approx 10^{15}$ cm^{-2}, Vidal-Madjar et al. 1994). The very presence of CO may also need a permanent replenishment naturally provided by evaporation of comet-like bodies.

We can evaluate the total mass of dust M_d which is associated with the evaporation of CO:

$$M_d = M_{co}\varphi\psi_{dust/gas}\psi_{gas/CO}\frac{t_d}{t_{CO}} \tag{12}$$

where M_{CO} is the total mass of CO in the disk, $\psi_{dust/gas}$ and $\psi_{gas/CO}$ are the mass ratios of dust to gas and gas to CO, φ is the mass ratio of the dust produced effectively kept in the disk and t_d and t_{CO} are the life time of dust and CO: due to photodissociation by UV interstellar radiation $t_{CO} \sim 300$ years (Vidal-Madjar et al. 1994), and at a distance of 100 AU where CO begins to be vaporized, $t_d \sim 10^6$ years (Backman & Paresce 1993). From the upper limit to particle size ($\beta \geq 0.4$), one can evaluate $\varphi \sim 0.1$. With a simple geometry of a disk with an opening angle of 10^o, we can deduce from the observed CO column density a total CO mass of about $M_{co} \approx 2 \cdot 10^{20}$ kg. From observations in the Solar System, we can take $\psi_{dust/gas} \geq 0.1$ (Newburn & Spinrad 1989). Finally, $\psi_{gas/CO}$ depends on the composition of the evaporated gas; it is between 1. if only CO is present and $\sim 10.$ if all volatiles evaporate (Mumma et al. 1993). Thus, with $\varphi\psi_{dust/gas}\psi_{gas/CO} \approx 0.1$, M_d is about one lunar mass, that is of the same order as the total mass of the dust disk independently evaluated!

This rough calculation shows that CO and dust are compatible with a common origin and produced by the same process: evaporation of comet-like bodies at large distances from the star.

5. Conclusion

The model we have proposed is able to account for the main characteristics of the β Pictoris disk as natural consequences of the production of secondary origin particles by small bodies. It is in fact an answer to the question 3 of Zuckerman & Becklin (1993): are the dust grains primordial or continually replenished?

Indeed, we have shown that if bodies produce dust particles with a given size distribution, these particles follow very eccentric orbits. Thus, a disk can be seen at large distances from the star, and the spatial distribution of dust is very close to a power-law. Moreover, the particles have the same inclinations as the parent bodies: the thickness of the disk thus increases with radius, and the disk is a "wedge" disk: (issue 4). The asymmetric spatial distribution can be explained if we assume that the parent bodies distribution is not axisymmetric (issue 2). This assumption is not surprising since asymmetry is observed for the FEBs and is probably the case in the Solar System for Kuiper belt objects trapped in planetary resonances (Jewitt & Luu 1995). Since particles are produced with periastrons greater than or equal to those of the parent bodies, the dust present close to the star is either produced there or brought in by Poynting-Robertson drag: the central part must be relatively clear (issue 3). Finally, this model gives connection between the particle size and their distances from the central star, and enable us to solve the issue of the disk mass (issue a), Section 4.4). Thus, the issues 2), 3), 4) and a) listed in Section 1 are simultaneously solved with the simplest form of the model presented here.

However, in order to explain the flatter gradient observed in the β Pictoris disk than the one obtained without additional hypothesis, we propose to add two other assumptions:
1) The dust is produced by evaporation of bodies of few kilometers in radius, so that there is a balance between evaporating gas drag and gravitation of these parent bodies, and only the smallest particles are extracted.
2) These bodies are moving slowly towards β Pictoris, so that they become extinct before arriving close to the star where the evaporating rate is large enough to produce the largest particles.
This OEB (Orbiting-Evaporating-Bodies) scenario is proposed to solve issue 1), but surprisingly it is also able to explain the abrupt change in the slope by the cutoff in distribution of particle size (issue 5)). It has to be noted that the cutoff must not necessary be very sharp and in fact is rather smooth in the model since we assumed a parent body size distribution. The model gives also a natural connection between the dust and gas disks (issue b): they may well be produced by the same bodies in the same process. The connection between the FEB and asymmetry in the disk seems to be possible (issue c)), however this point needs further analysis.

This new model is able for the first time to explain simultaneously these issues, but we must now ask if other models or hypothesis can also be made with the same consequences. If correct, this OEB scenario allows to see the β Pictoris disk as a gigantic multi-cometary tail with all its components: gas and dust.

Acknowledgements. We would like to express our gratitude to Dr. F.Roques who first recall us that ejected particles follow peculiar eccentric orbit. We are particularly indebted to the anonymous referee for his very useful comments which substantially improved the paper. Our thanks go also to Dr. M. Friedjung for improving the manuscript.

References

Artymowicz P., 1988, ApJL 335, L79
Artymowicz P., Burrows C., Paresce F., 1989, ApJ 337, 494
Artymowicz P., Paresce F., Burrows C., 1990, Adv. Space Res. 10, (3)81
Aumann H.H., Gillett F.C., Beichman C.A. et al., 1984, ApJ 278, L23
Backman D.E., Gillett F.C., Witteborn F.C., 1992, ApJ 385, 670
Backman D.E., Paresce F., 1993, in *Protostars and Planets III*, Eds. E.H. Levy, J.I. Lunine & M.S. Matthews (Tuscon: Univ. Arizona Press), p 1253
Beust H., Vidal-Madjar A., Ferlet R., Lagrange-Henri A.M., 1991, A&A 241, 488
Burns J., Lamy P., Soter S., 1979, Icarus 40, 1
Cowan J.J., A'Hearn M.F., 1982, Icarus 50, 53
Fernández J.A., 1982, A.J. 87, 1318
Freudling W., Lagrange-Henri A.M., Vidal-Madjar A., Ferlet R., Forveille T., 1995, A&A, in press
Fujiwara A., Cerroni P., Davis D. et al., 1989, Asteroid II, Eds Binzel R.P., Gehrels T. & Matthews M.S. (Tucson: Univ. of Arizona Press), p 240.
Golimowski D.A., Durrance S.T., Clampin M., 1993, ApJ 411, L41
Gombosi T.I., Cravens T.E., Nagy A.F., 1985, ApJ 293, 328
Greenberg R., Nolan M.C., 1989, Asteroid II, Eds Binzel R.P., Gehrels T. & Matthews M.S. (Tucson: Univ. of Arizona Press), p 778.
Hughes D.W., Daniels P.A., 1982, MNRAS 198, 573
Jewitt D.C., Luu J.X., 1995, AJ 109, 1867
Kallas P., Jewitt D., 1995, Proceedings of the 10th IAP Astrophysics Meeting, Eds. R.Ferlet & A.Vidal-Madjar (Editions Frontieres)
Lagage P.O., Pantin E., 1994, Nature 369, 628
Lecavelier Des Etangs A., Perrin G., Ferlet R., et al., 1993, A&A 274, 877
Lecavelier des Etangs, A., Deleuil M., Vidal-Madjar A., et al., 1995, A&A 299, 557
Le Sergeant L.B., Lamy P.L., 1980 Icarus 43, 350
Levison H.F., 1991, AJ 102, 787
Lien D.J., 1990, ApJ 355, 680
Lissauer J.J., 1993, Ann. Rev. Astron. Astrophys. 31, 129
Luu J.X., Jewitt D.C., 1990, AJ 100, 913
Mumma M.J., Weissman P.R., Stern S.A., 1993, in *Protostars and Planets III*, Eds. E.H. Levy, J.I. Lunine & M.S. Matthews (Tuscon: Univ. Arizona Press), p 1177

Nakano T., 1990, ApJL 355, L43
Newburn R.L., Spinrad H., 1989, AJ 97, 552
Paresce F., Burrows C., 1987, ApJL 319, L23
Paresce F., 1991, A&A 247, L25
Scholl H., 1979, Icarus 40, 345
Sekanina Z., 1987, A&A 187, 789
Smith B.A., Terrile R.J., 1984, Sci 226, 1421
Smith B.A., Terrile R.J., 1987, BAAS 19, 829
Torbett M.V., Smoluchowski R., 1990, Nat. 345, 49
Vidal-Madjar A., Hobbs L.M., Ferlet R., Gry C., Albert C.E., 1986, A&A 167, 325
Vidal-Madjar A., Lagrange-Henri A.M., Feldman P.D. et al., 1994, A&A, 290, 245
Vidal-Madjar A., Ferlet R., 1995, in *Circumstellar Dust Disks and Planet Formation*, Proceedings of the 10th IAP Astrophysics Meeting, Eds. R.Ferlet & A.Vidal-Madjar (Editions Frontieres), in press
Weissman P.R., 1984, Science 224, 987
Whipple F.L., 1975, A.J. 80, 525
Zuckerman B., Becklin E.E., 1993, ApJ 414, 793

This article was processed by the author using Springer-Verlag LaTeX A&A style file *L-AA* version 3.